Monthly Notices of the ROYAL ASTRONOMICAL SOCIETY

MNRAS **441,** 900–909 (2014) doi:10.1093/mnras/stu553

Intermediate-mass black holes in AGN discs – II. Model predictions and observational constraints

B. McKernan,[1,2,3,4★] K. E. S. Ford,[1,2,3,4] B. Kocsis,[5,6] W. Lyra[7,8†] and L. M. Winter[9]

[1]*Department of Science, Borough of Manhattan Community College, City University of New York, New York, NY 10007, USA*
[2]*Department of Astrophysics, American Museum of Natural History, New York, NY 10024, USA*
[3]*Graduate Center, City University of New York, 365 5th Avenue, New York, NY 10016, USA*
[4]*Kavli Institute for Theoretical Physics, UC Santa Barbara, CA 93106, USA*
[5]*Harvard–Smithsonian Center for Astrophysics, 60 Garden St, Cambridge, MA 02138, USA*
[6]*Institute for Advanced Study, Einstein Drive, Princeton, NJ 08540, USA*
[7]*Jet Propulsion Laboratory, California Institute of Technology, 4800 Oak Grove Dr., Pasadena, CA 91109, USA*
[8]*California Institute of Technology, Division of Geological & Planetary Sciences, 1200 E. California Blvd, Pasadena, CA 91125, USA*
[9]*Center for Astrophysics & Space Astronomy, University of Colorado, Boulder, CO 80303, USA*

Accepted 2014 March 17. Received 2014 January 28; in original form 2012 September 24

ABSTRACT

If intermediate-mass black holes (IMBHs) grow efficiently in gas discs around supermassive black holes, their host active galactic nucleus (AGN) discs should exhibit myriad observational signatures. Gap-opening IMBHs in AGN discs can exhibit spectral features and variability analogous to gapped protoplanetary discs. A gap-opening IMBH in the innermost disc imprints ripples and oscillations on the broad Fe Kα line which may be detectable with future X-ray missions. A non-gap-opening IMBH will accrete and produce a soft X-ray excess relative to continuum emission. An IMBH on a retrograde orbit in an AGN disc will not open a gap and will generate soft X-rays from a bow-shock 'headwind'. Accreting IMBH in a large cavity can generate ULX-like X-ray luminosities and LINER-like optical line ratios from local ionized gas. We propose that many LINERs house a weakly accreting MBH binary in a large central disc cavity and will be luminous sources of gravitational waves (GW). IMBHs in galactic nuclei may also be detected via intermittent observational signatures including: UV/X-ray flares due to tidal disruption events, asymmetric X-ray intensity distributions as revealed by AGN transits, quasi-periodic oscillations and underluminous Type Ia supernovae. GW emitted during IMBH inspiral and collisions may be detected with *eLISA* and LIGO, particularly from LINERs. We summarize observational signatures and compare to current data where possible or suggest future observations.

Key words: accretion accretion discs – planets and satellites: formation – planet-disc interactions – protoplanetary discs – galaxies: active – galaxies: Seyfert.

1 INTRODUCTION

There is overwhelming observational evidence for supermassive black holes (SMBH; $>10^6\,M_\odot$) in the centres of galaxies (Kormendy & Richstone 1995) and stellar mass BHs ($<20\,M_\odot$) in our own Galaxy (Remillard & McClintock 2006). However, there is only fragmentary evidence for intermediate-mass black holes (IMBHs, see Davis et al. 2011 for the best candidate to date). IMBHs are thus a key missing component of our Universe. The standard model of IMBH production is in clusters (Miller & Hamilton 2002); however, there are currently no undisputed cases of IMBHs in globular clusters (Strader et al. 2012); IMBHs are hard to find.

In McKernan et al. (2012, Paper I), we described a model for the production and growth of IMBH seeds in discs around SMBH. Our model grows IMBH seeds at super-Eddington rates in discs in active galactic nuclei (AGN). IMBH growth occurs both via collision of stars and compact objects at low relative velocity in discs (core accretion) and via gas accretion as the IMBH migrates within the disc. Our model is analogous to the growth of giant planets in protoplanetary discs (e.g. Pollack et al. 1996; Armitage 2010) and grows IMBHs more efficiently than the standard model (Miller & Hamilton 2002). In this paper, we outline the wide range of predicted observables that can reveal IMBHs in galactic nuclei throughout the local Universe.

In Section 2, we discuss conditions in the AGN disc under which IMBHs can open a gap. In Section 3, we discuss observational consequences of gaps in the outer AGN disc. We draw a parallel

★ E-mail: bmckernan@amnh.org
† Sagan Fellow.

between observational signatures of gapped protoplanetary discs and gaps carved out by IMBHs in AGN discs. In Section 4, we outline the effect of a gap-opening IMBH in the inner AGN disc on the broad component of the Fe Kα line, which yields signatures that allow us to follow the final stage of mergers and provides advance warning of gravitational wave (GW) outbursts. In Section 5, we discuss the signatures of accreting IMBHs in AGN discs. In Section 6, we discuss occasional signatures of IMBHs in galactic nuclei. In Section 7, we discuss GW signatures of our model potentially detectable with LIGO and *LISA*.

2 GAP OPENING IN AGN DISCS

Gap opening in any accretion disc depends on the ratio of satellite mass (M_2) to primary mass (M_1), disc viscosity and the disc aspect ratio. A simple estimate of the critical mass ratio ($q = M_2/M_1$), above which the IMBH will open a gap in the disc, is given by (Lin & Papaloizou 1986)

$$q \approx \left(\frac{27\pi}{8}\right)^{1/2} \left(\frac{H}{r}\right)^{5/2} \alpha^{1/2}, \quad (1)$$

where (H/r) is the disc thickness and α is the viscosity parameter (Shakura & Sunyaev 1973). The pre-factor can differ by up to an order of magnitude depending on the approximations used in calculating the torque (Crida, Morbidelli & Masset 2006); however, for most of the disc models equation (1) is sufficient to estimate the minimum gap-opening mass (Edgar, Quillen & Park 2007). Clearly, only IMBH or larger mass BH can open gaps in AGN discs. In particular, to open a gap requires low disc viscosity such that (Crida et al. 2006)

$$\alpha < 0.09 q^2 \left(\frac{H}{r}\right)^{-5}. \quad (2)$$

Even if an IMBH is sufficiently massive to open a gap in a disc ($q > 10^{-4}$ typically), the gap can close by pressure if the disc is geometrically thick enough such that (Bryden et al. 1999)

$$\frac{H}{r} > \frac{1}{40}\left(\frac{q}{\alpha}\right)^{1/2}. \quad (3)$$

Combining these conditions allows gap opening to occur when $H/r \lesssim \min[(1/40)(q/\alpha)^{1/2}, (q^2/\alpha)^{1/5}]$. Thus, any gap detection can tell us a lot about AGN discs. We do not address in detail the recent result from Zhu, Stone & Rafikov (2013) that low-mass satellites may open gaps in a disc but note that in hot AGN discs even IMBH with $q < 10^{-4}$ may open gaps.

Just before gap opening occurs, the disc perturbation may allow for very rapid type III migration (Masset & Papaloizou 2003; Pepliński, Artymowicz & Mellema 2008a,b) with consequences for observed AGN luminosity (McKernan et al. 2011b). Once a gap opens, the outer edge of the gap is exposed to the central radiation source and both the inner edge and the disc immediately outside the outer edge are shadowed, leading to a change in the observed spectral energy distribution (SED; e.g. Jang-Condell & Sasselov 2003; Espaillat et al. 2007; and see Section 3 below). The gap will be approximately $2R_{\rm H}$ in width where $R_{\rm H} = a(q/3)^{1/3}$ is the IMBH Hill radius and a the IMBH semimajor axis. The gap is not completely empty as the IMBH is fed by leading and trailing resonance arms (analogous to gap-opening Jupiters in protoplanetary discs) and the IMBH may have an accretion disc of size-scale $R \ll R_{\rm H}$ (Hayasaki, Mineshige & Ho 2008; Roedig et al. 2012; D'Orazio, Haiman & MacFadyen 2013). A gap-opening IMBH migrates within the disc on the so-called type II migration time-scale given by

$$\tau_{\rm II} = \frac{1}{\alpha}\left(\frac{H}{r}\right)^{-2}\frac{1}{\omega}, \quad (4)$$

where ω is the Keplerian angular frequency and $\tau_{\rm II} = \tau_\alpha$, the viscous disc time-scale.

The co-evolution of an AGN disc with an IMBH can differ from that of planets in a protoplanetary disc. First, the type II migration rate varies depending on the ratio of the gas to radiation pressure in the inner AGN disc, since this influences (H/r) and α. Secondly, the mass of the IMBH may be larger than the local disc mass in the radiation-pressure-dominated regime. In this case, the disc banks up on the outer edge of the gap before it can push the IMBH inwards (Syer & Clarke 1995; Ivanov et al. 1999; Kocsis, Haiman & Loeb 2012a). The viscous time-scale is smallest inside the orbit of the IMBH, so the inner disc can drain away, leaving an empty central cavity (Artymowicz & Lubow 1996; Kocsis, Haiman & Loeb 2012b). The viscous disc will pile up just outside the IMBH orbit, analogous to the build-up of water behind a dam. The dam may leak or burst after a time, refilling the inner disc and leaving an annulus in the disc and/or an accreting IMBH (e.g. Kocsis et al. 2012a; McKernan et al. 2013; D'Orazio et al. 2013; Farris et al. 2014, and references therein). Thirdly, GW emission by the IMBH eventually dominates over type II migration. If there is a circular cavity in the disc, once the GW time-scale becomes shorter than the viscous time, the outer edge of the gap cannot follow the IMBH and effectively freezes until the binary merges (Armitage & Natarajan 2002; Liu, Wu & Cao 2003; Milosavljevic & Phinney 2005). However, if there is an inner disc as the IMBH inspirals due to GW emission, the gap may retain an annular geometry with characteristic width $\sim R_{\rm H}$ tracking the inspiralling IMBH (Baruteau, Ramirez-Ruiz & Masset 2012, see however Chang et al. 2010). Only IMBH or SMBH can open gaps in AGN discs, so the detection of gaps in discs will set excellent constraints on (H/r), α in models of AGN discs (Ivanov et al. 1999; Hayasaki et al. 2008; Kocsis et al. 2012a; Rafikov 2013), in spite of uncertainties in those models.

3 GAPS AND CAVITIES IN OUTER AGN DISCS: PREDICTIONS

Our model of IMBH growth displays strong parallels with models of giant planet growth in protoplanetary discs. A large fraction ($>1/5$) of protoplanetary discs exhibit evidence for gaps or cavities probably carved out by giant protoplanets (e.g. Andrews et al. 2011, and references therein). If AGN disc conditions permit an IMBH to carve out a gap or cavity, the AGN should display features and variability analogous to those in gapped protoplanetary discs.

3.1 SED dip: predictions

Consider an AGN disc consisting of annuli, each at a different temperature. In an AGN disc without a gap, each of the annuli contributes a blackbody spectrum to the overall multicolour optical/UV spectrum. If the AGN disc includes a gap, then the blackbody spectrum due to that missing annulus is subtracted from the overall spectrum, leading to a dip or break around that disc temperature (Gültekin & Miller 2012), independent of breaks due to reddening or absorption edges (e.g. Zheng et al. 1995). From protoplanetary disc theory, the width of the gap (w) will be $w \geq 2R_{\rm H} = 2(q/3)^{1/3}a \sim 0.07(0.14)a$, for $q = 10^{-4}(10^{-3})$ (Armitage 2010), where a is the semimajor axis of the IMBH orbit.

The spectral break wavelength (λ_b) due to a fully empty blackbody annulus in a homogeneous thin disc around an SMBH of mass M accreting at rate $\dot{M}$ is

$$\lambda_b = \left(\frac{hc}{xk}\right)\left(\frac{G}{2\pi\sigma}\right)^{-1/4}\left(\frac{M\dot{M}}{r^3}\right)^{-1/4}, \quad (5)$$

where $x \sim 5$, and we rewrite λ_b as

$$\lambda_b \sim 140\eta^{1/4}\left(\frac{r_2}{r_g}\right)^{3/4}\left(\frac{M_1}{10^8\,M_\odot}\right)^{1/4}\left(\frac{\dot{m}}{0.01}\right)^{-1/4}\text{Å}, \quad (6)$$

where r_2 is the location of the gap (in units of $r_g = GM_1/c^2$), M_1 is the mass of the primary SMBH, $\dot{m}$ is the Eddington accretion ratio ($\dot{m} = 1.0$ is the Eddington rate) and η is the accretion efficiency ($\eta = 0.06 - 0.42$ for the full range of BH spins). Thus, a gap at $10^3 r_g$ in a thin homogeneous disc around a $10^6(10^8)\,M_\odot$ SMBH leads to a break at $\lambda_b \sim 0.4(1.4)(\eta/0.1)^{1/4}$ μm. Equation (6) can be compared directly with equation 13 in Gültekin & Miller (2012), with our pre-factor agreeing with theirs (∼140) for $\eta \sim 0.1$ if their $f(w/h) \sim 0.6$. A sufficiently wide gap leads to a broad dip in the broad-band optical continuum (see e.g. fig. 1 in Gültekin & Miller (2012) for an illustration, although their break should be located around ∼ 2 μm not ∼ 0.2 μm). Local disc mass is expected to decrease rapidly at small radii, so we should observe deeper and wider spectral dips in the SED as λ_b decreases.

Assuming the irradiated outer disc flares, such that H/r is an increasing function of radius, the blackbody temperature of the irradiated outer gap wall (T_{wall}) is given by (Armitage 2010)

$$T_{wall} = L_{inner}^{1/4}\theta^{1/4}r_{wall}^{-1/2}, \quad (7)$$

where L_{inner} is the AGN luminosity due to material at $r < r_{wall}$ and $\theta = -H_r/r + dH_r/dr$ is the angle between the continuum source and the tangent to the disc surface and $H_r \sim H$ the disc thickness in the limit of a very optically thick disc. Rewriting in terms of $\dot{m}$, M_1, we find that the peak wavelength of outer gap emission is

$$\lambda_{wall} \approx 165\left(\frac{r_2}{r_g}\right)^{1/2}\left(\frac{M_1}{10^8\,M_\odot}\right)^{1/4}\left(\frac{\dot{m}}{0.01}\right)^{-1/4}\theta^{-1/4}\text{Å}, \quad (8)$$

where θ may be rewritten in terms of the opening angle of the disc at the wall (β) and radius of the inner accretion disc r_{in} as $\theta^{-1/4} \approx (\cos\beta/4)^{1/4}(r_{in}/r_{wall})^{1/2}$. In a (more realistic) flared disc, λ_b due to the gap is found from the $r^{-1/2}$ dependence in equation (8) rather than the $r^{-3/4}$ dependence in equation (6). Thus, a gap at $10^3 \pm 10^2 r_g$ in a flared disc around a $10^6(10^8)\,M_\odot$ SMBH yields a break centred on $\lambda_b \sim 0.06(0.22)(\theta/30)^{-1/4}$ μm and a corresponding bump due to the wall at $\lambda_{wall} \sim 1.05 \times \lambda_b$.

In the gas-pressure-dominated region of the disc, the outer wall height can be approximated by (Armitage 2010)

$$H_{wall} \approx \frac{c_s}{\omega} = \left(\frac{k_B}{\mu m_p}\right)^{1/2} T_{wall}^{1/2}\omega^{-1}, \quad (9)$$

where c_s is the sound speed (see Kocsis et al. 2012b, for the radiation-pressure-dominated case). The maximum luminosity of the outer wall can be approximated by $L_{wall,\,max} \approx (H_{wall}/r)L_{inner}/4$. Shadowing by the inner disc will reduce the observed value of L_{wall}. For $H_{wall}/r \sim 0.1$, then $L_{wall} \leq 3$ per cent L_{inner}.

In certain cases, a cavity will form in the AGN disc rather than a gap. When the local disc mass $< M_2$, secondary migration will stall (e.g. Syer & Clarke 1995; Kocsis et al. 2012a; McKernan et al. 2013). As the inner disc drains 'inside-out', gas will pile up at the outer gap edge and a cavity can form (McKernan et al. 2013). As the inner disc drains to form a cavity, L_{inner} decreases. Since our model predicts that in flared discs with gaps/cavities,

$$\lambda_{wall} \approx 140\left(\frac{L_{inner}}{10^{43}\,\text{erg s}^{-1}}\right)^{-1/4}\left(\frac{\theta}{30}\right)^{-1/4} \times \left(\frac{r}{r_g}\right)^{1/2}\left(\frac{M_1}{10^8\,M_\odot}\right)^{1/2}\text{Å} \quad (10)$$

for $L_{inner} \sim 10^{42(43)}$erg s^{-1}, $\lambda_{wall} \sim 0.8(0.4)$ μm at $10^3 r_g$. Our model predicts that while L_{inner} decreases, the SED slope at $\lambda \geq \lambda_{wall}$ steepens due to continued viscous gas inflow and pile-up as L_{wall} increases. Thus, in discs with gaps/cavities, our model predicts an anticorrelation between average L_{inner} and the SED slope at $\lambda \geq \lambda_{wall}$. This prediction distinguishes our model from models of cavity formation due to inner disc instability and collapse, since there is no (or little) pile-up in the latter case. Interestingly, pile-up at the outer gap edge will generate a luminous annulus in the disc, which may be detectable in an optical stellar transit of the AGN disc (see Section 6.1 below).

As the inner disc drains inside-out, regions of short time-scale variability are removed from the AGN disc. Gas pile-up on the viscous time-scale ($\tau_\alpha(r_{wall})$) will be accompanied by disc drainage on much faster inner disc time-scales. Thus, our model predicts that a decline in power on short time-scales in the power density spectrum (PDS) of an AGN, due to removal of the inner disc, will be accompanied by a prominent peak in the PDS due to variation on the characteristic pile-up time-scales. If we approximate the gas pile-up on the gap/cavity edge as an unstable, thick advective flow (particularly as photoionization declines), the time-scale of variability (Δt_{wall}) of such a flow is roughly the free-fall time-scale

$$\Delta t_{wall} \geq 16\left(\frac{M_1}{10^8\,M_\odot}\right)\left(\frac{r_{wall}}{100r_g}\right)^{3/2}\text{d}, \quad (11)$$

which is comparable to observed prominent breaks on time-scales of ∼ 5−100 d in AGN PDSs (e.g. Collier & Peterson 2001). Even if the pile-up is unstable on short times and leaks completely into the gap/cavity, refilling the disc, torques from the secondary can still excavate a new gap/cavity in the disc and the cycle begins again.

The dam wall that holds back the piled-up gas may be leaky at best and not endure for long, particularly at high accretion rates (see McKernan et al. 2013, for extensive discussions). In the case of high accretion rates, cavities may be short lived and quickly refilled as stalled gap-opening migration resumes. Cavities will only persist until mass $\geq M_2$ builds up at the cavity edge, so the cavity lifetime is $\tau_{cav} \geq M_2/\dot{M}_1$. The AGN disc lifetime is given by $\tau_{disc} = q_{disc}M_1/\dot{M}_1$, so among discs with IMBH, a fraction $\tau_{cav}/\tau_{disc} = q_2/q_{disc}$ will exhibit cavities where $q_2 = M_2/M_1$ and $q_{disc} = M_{disc}/M_1$. Thus, if an AGN disc ($q_{disc} \sim 10^{-2}$) hosts a sufficiently massive IMBH ($q_2 \sim 10^{-4}$), it has about a 1 per cent chance of being observed with a cavity.

Discs around lower mass SMBH are the likeliest observational targets for finding gaps or cavities. Around low-mass SMBH, note that even large mass (short-lived) stars could maintain a cavity in the inner disc for most of their main-sequence lives. Around an SMBH with $M_1 = 10^6\,M_\odot$, an AGN disc lasts $\tau_{disc} \sim 50(q_{disc}/10^{-2})(\eta/0.1)(M_6/10^6\,M_\odot)(\dot{m}_1/0.01)^{-1}$ Myr, where $\dot{m}_1$ is the Eddington ratio of the primary. An $M_2 = 10\,M_\odot$ stellar mass BH growing in this disc at $\dot{m}_2 \sim 3.5\times$ Eddington via collisions and gas accretion reaches gap/cavity opening threshold ($q_2 \sim 10^{-4}$, $M_2 \sim 100\,M_\odot$ in time $\tau_{gap} \sim 35(\dot{m}_2/3.5)$ Myr (McKernan et al. 2012). Assuming that every low-mass AGN disc starts off with a stellar mass BH, if $\tau_{gap} < \tau_{disc}$, a crude estimate

of the probability of a gap or cavity in discs around $M_1 \sim 10^6\,\mathrm{M}_\odot$ SMBH is $P_{\rm gap} = 1 - (\tau_{\rm gap}/\tau_{\rm disc})$ or

$$P_{\rm gap} = 1 - \left[0.7\left(\frac{\dot{m}_2}{3.5}\right)\left(\frac{10^{-2}}{q_{\rm disc}}\right)\left(\frac{0.1}{\eta}\right)\left(\frac{10^6\,\mathrm{M}_\odot}{M_6}\right)\left(\frac{\dot{m}_1}{0.01}\right)\right]. \quad (12)$$

A more detailed estimate can be constructed by accounting for the location of M_2, the local mass supply and Bondi accretion (Kocsis, Yunes & Loeb 2011; Ju et al. 2013). Thus, around low-luminosity Seyfert AGN with $M_1 \sim 10^6\,\mathrm{M}_\odot$, we expect $\sim$1/3 of discs to display evidence of gaps and only $\sim$1 per cent to display evidence for cavities. If IMBH in AGN discs start from stellar mass BH seeds, then only $\sim$1 per cent of higher luminosity Seyfert AGN will display evidence for gaps and little or no evidence for cavities due to IMBH formed in the disc. However, if IMBH survive the AGN phase, they can grow much larger in subsequent phases and a larger fraction of higher luminosity and higher mass AGN may display evidence for gaps and cavities. At $z < 0.1$, there are tens of well-studied X-ray-selected Seyfert AGN including $\sim$10 low-mass Seyferts. Several of these AGN (e.g. MCG-6-30-15) are heavily absorbed in the optical/UV, so it is difficult to constrain optical accretion discs in these cases. A systematic survey of hundreds of optically selected AGN will yield the strongest statistical constraints on the occurrence of gaps and cavities in AGN discs. If, after accounting for reddening and naturally occurring spectral breaks (e.g. Zheng et al. 1995), there is an absence of breaks in the 'big blue bump' of AGN SEDs, we can rule out the presence of close MBH mergers in AGN and severely restrict models of IMBH in AGN discs.

3.2 Predictions from a parallel with gapped protoplanetary discs

The previous section is based on physical expectations but we can also make predictions by analogy, based on observations of gapped protoplanetary discs. First, some emission lines in protoplanetary discs are observed to be double-peaked due to the presence of a gap or cavity, which leads to blue- and redshifted peaks in the line emission (Andrews et al. 2011). By analogy, our model predicts double-peaked low-ionization optical/UV line profiles in AGN. A small fraction of AGN are indeed observed to display double-peaked low-ionization emission lines (Strateva et al. 2003; Lewis, Eracleous & Storchi-Bergmann 2010). These lines and their variability (Lewis et al. 2010) can be accounted for by a gap-opening IMBH trailed and led by clumpy spiral density waves. Double-peaked lines observed in NGC 4151 for example, could be explained by a BH binary, with a large mass secondary ($q \sim 0.01$–0.1) at large eccentricity (Bon et al. 2012). Our model predicts that double-peaked lines must originate outside the disc cavity, so a spectral break or dip in the SED must occur at $\lambda_{\rm b} < \lambda_L$, the line wavelength. We can test this prediction in the sample of AGN with double-peaked lines, by comparing the time-scales of variability of the double-peaked lines ($t_{\rm l}$) with the time-scale of variability of the outer gap wall ($t_{\rm wall}$). If $t_{\rm l} \leq t_{\rm wall}$, then our interpretation of these lines must be incorrect.

Secondly, in protoplanetary discs, the outer gap/cavity wall is directly exposed to the stellar ionizing continuum and emits a blackbody at $\lambda_{\rm wall}$ with luminosity proportional to the wall height (Andrews et al. 2011), followed by a luminosity drop at $L(\lambda > \lambda_{\rm wall})$ due to shadowing by the wall. Our model predicts the same basic observable: a prominent blackbody peak in the AGN SED at $\lambda_{\rm wall}$, with $L(\lambda > \lambda_{\rm wall}) < L(\lambda_{\rm wall})$ due to shadowing. The luminosity at $\lambda_{\rm wall}$ varies on time-scale $\Delta t_{\rm wall}$ which will be significantly faster than the time-scale of variability at $\lambda > \lambda_{\rm wall}$.

Thirdly, in the SEDs of gapped protoplanetary discs, as $L(\lambda < \lambda_{\rm wall})$ increases, $L(\lambda > \lambda_{\rm wall})$ is observed to decrease, and vice versa (Espaillat et al. 2007). This 'see-saw' variability is believed to be due to occasional puffing up of the inner disc (short wavelengths), shadowing the outer disc wall (long wavelengths). By analogy, our model predicts exactly this sort of spectral variability in gapped AGN discs. We predict that during a flaring high state in X-rays from the innermost disc, $L(\lambda < \lambda_{\rm wall})$ due to the irradiated inner disc must increase. Since the puffed-up inner disc shadows the outer gap, $L(\lambda_{\rm wall})$ must decrease. Conversely, during an AGN 'low state' where $L_{\rm x}$ diminishes, $L(\lambda < \lambda_{\rm wall})$ will also decrease, but $L(\lambda_{\rm wall})$ must increase as the outer gap/cavity wall is no longer shadowed by the puffed-up inner disc. Thus, in sources that are X-ray luminous (i.e. with a substantial inner disc), but with high flaring or low states, our model predicts a linear correlation between $L_{\rm x}$ and $L(\lambda < \lambda_{\rm wall})$, but an anticorrelation between $L_{\rm x}$ and $L(\lambda_{\rm wall})$.

3.3 LINERs as AGN discs with cavities

A sub-class of galactic nuclei, LINERs, do not exhibit a prominent blue/UV bump in their SEDs (e.g. Maoz et al. 2005; Ho 2008). Thus, either LINERs do not have a prominent thermal disc or the accretion flow is radiatively inefficient. If there is no accretion disc, photoionization could be powered by asymptotic giant branch stars (e.g. Eracleous, Hwang & Flohic 2010). We suggest an alternative possibility. In our model, a substantial cavity carved out by an IMBH (or SMBH) can account for the absence of a prominent disc signature. By removing the inner disc to large radii, the reduced ionizing continuum luminosity will change the optical line ratio from AGN-like. If the massive binary in the cavity is accreting weakly due to a leaky dam (see Section 2), the ionizing continuum will have a much lower luminosity, akin to LLAGN or an ultraluminous X-ray source (ULX), and therefore, the observed line ratios must be LINER-like (McKernan et al. 2011a). ULXs (which may be powered by accretion on to IMBH) have now been observed with optical line ratios remarkably consistent with those in LINERs and LLAGN (Berghea & Dudik 2012). Thus, our model predicts that many LINERs consist of MBH binaries in large central cavities in a gas disc. A small fraction of these LINERs will be GW loud (depending on $a_{\rm bin}$).

Specifically, our model predicts: (1) a rise in the optical spectrum of LINERs due to the cavity wall at $\lambda_{\rm wall}$, together with (2) an immediate dip at $\lambda > \lambda_{\rm wall}$ due to pile-up and disc shadowing of a weakly accreting central source, (3) significantly shorter variability time-scales at $L(\lambda_{\rm wall})$ compared to $L(\lambda > \lambda_{\rm wall})$, (4) little or no power in the LINER PDS on time-scales $< t_{\rm wall}$ and (5) double-peaked low-ionization lines at $\lambda > \lambda_{\rm wall}$. In this model, the IMBH/SMBH occupy a substantial cavity. If the cavity is not leaky, the binary will not accrete strongly. Such LINERs will not exhibit a prominent, luminous, soft X-ray excess (see Section 5 below). However, if the cavity is leaky, accretion on to the IMBH/secondary MBH could dominate the accretion on to the SMBH yielding ULX-like optical line ratios.

4 GAPS AND CAVITIES IN INNER AGN DISCS: PREDICTIONS

In the limit of small disc radii, as a gap-opening IMBH migrates closer to the SMBH, the gap in the accretion disc can imprint itself on the broad component of the Fe Kα line profile (see McKernan

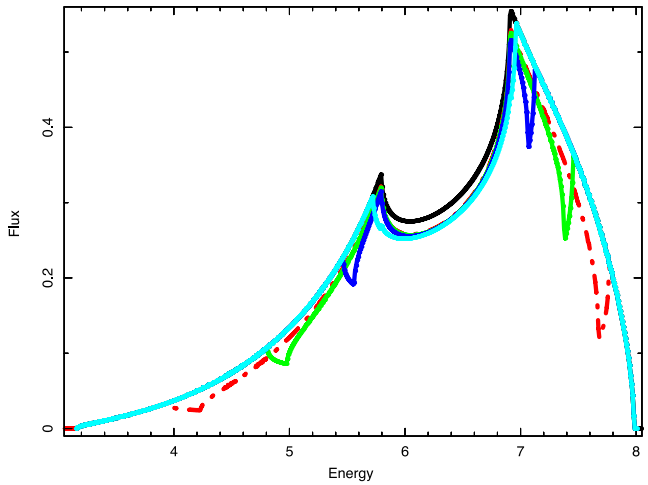

Figure 1. The change in Fe Kα profile for the in-migration of a $q = 3 \times 10^{-3}$ IMBH across the inner disc with empty gap of width $2R_{\rm H}$ where $R_{\rm H} = (q/3)^{1/3}R$. Flux is in normalized arbitrary units and energy is in units of keV. Solid black line indicates the unperturbed Fe Kα profile. Turquoise solid line denotes an annulus at $90 \pm 9r_{\rm g}$ in the inner disc. Dark blue solid line denotes an annulus at $50 \pm 5r_{\rm g}$, Green solid line corresponds to an annulus at $20 \pm 2r_{\rm g}$ and the dashed red line corresponds to an annulus at $10 \pm 1r_{\rm g}$. See McKernan et al. (2013) for detailed discussion of this and other effects in the broad Fe Kα line as well as detectability with future missions.

et al. 2013, for extensive discussion). Fig. 1 illustrates the simulated, noiseless variation in a broad Fe Kα line profile due to an in-migrating empty annulus (occupied by an IMBH) of width $2R_{\rm H}$ (where $R_{\rm H} = (q/3)^{1/3}a$) and a is the circularized orbit radius) decreasing from $100r_{\rm g}$ to $6r_{\rm g}$. We calculated the broad Fe Kα line profile around a Schwarzschild BH using the `diskline` algorithm (Fabian et al. 1989). We assumed $q = 3 \times 10^{-3}$, the disc is inclined by 60^o to the observer's line of sight and the X-ray continuum goes as $r^{-2.5}$. As the IMBH and gap migrate into the inner $100r_{\rm g}$ of the disc, a flux deficit appears (turquoise solid line) compared to the unperturbed profile (black solid line). As inward migration continues, the empty gap removes flux from increasingly red and blue regions of the disc and the twin notches move apart, redward and blueward, respectively, from the line centre (6.4 keV). As the empty gap moves inwards in the disc from $50r_{\rm g}$ to $10r_{\rm g}$ (red curve), the blue notch moves from 6.5 out to 7.2 keV, and the red notch moves from 5.6 to 4.2 keV.

The time-scale to merger of an IMBH–SMBH binary via gravitational radiation is given by (Peters 1964)

$$\tau_{\rm GW} \approx 10^{12}\ {\rm yr} \left(\frac{10^3\,{\rm M}_\odot}{M_2}\right)\left(\frac{10^6\,{\rm M}_\odot}{M_1}\right)^2\left(\frac{a_{\rm bin}}{0.001\,{\rm pc}}\right)^4 (1-e^2)^{7/2}, \quad (13)$$

where M_2 is the mass of the secondary IMBH, M_1 is the mass of the primary SMBH, $a_{\rm bin}$ is the binary separation and e is the IMBH orbital eccentricity. For a $3000\,{\rm M}_\odot$ IMBH around a $10^6\,{\rm M}_\odot$ SMBH, the progression from green to red curve in Fig. 1 takes $\sim$16 yr and from red curve to final merger takes $\sim$1yr. Low-mass AGN exhibiting broad Fe Kα lines (e.g. MCG-6-30-15) have the shortest time-scales for merger and low-mass migrators (IMBH and stellar mass BH) in the inner disc are the most likely sources of a late-stage ripple effect (McKernan et al. 2013). Oscillations caused by e.g. an accreting secondary (IMBH) in a cavity around a primary SMBH can be readily tested with the proposed *LOFT* mission (see McKernan et al. 2013 for further details).

Future X-ray missions, such as *Astro-H* and *IXO-Athena*, have the energy resolution to distinguish between features due to highly ionized Fe (e.g. McKernan & Yaqoob 2004) and may detect the ripple signatures or oscillations. Observations of the latter stages of the ripple effect in the broad Fe Kα line of a low-mass AGN, predict a prompt rise in GW luminosity from this source, which should reach the threshold of future GW detectors. This signal therefore constitutes a prime EM precursor for GW observations.

5 EMBEDDED OBJECTS IN AGN DISCS: PREDICTIONS

In this section, we discuss the case of embedded objects in AGN discs, including IMBH that do not open a gap. In Section 5.1, we discuss the observational signatures of accreting embedded objects in the AGN disc. In Section 5.2, we discuss observational signatures due to embedded objects on retrograde orbits within the AGN disc. In Section 5.3, we examine whether one or other or both models could contribute to, or correspond wholly to the soft X-ray excess observed in many AGN.

5.1 Predictions from accretion

IMBH can accrete from the gas disc at up to Eddington rates (Nayakshin & Sunyaev 2007), although they can grow at super-Eddington rates including collisions in the disc (McKernan et al. 2013). A gas disc accreting on to an IMBH produces a blackbody spectrum peaking in the soft X-ray band at temperatures of $\sim$0.1 keV($10^4\,{\rm M}_\odot$)$-$1 keV($10^2\,{\rm M}_\odot$). This is observationally interesting because in many (possibly most) AGN, an excess of soft X-rays ($\sim$0.1–1.0 keV) is observed, relative to the level expected from extrapolating a power-law fit from hard X-rays (>1 keV) (e.g. Gierliński & Done 2004; Scott, Stewart & Mateos 2012). The excess is observed to have a quite remarkable constant temperature peak, independent of large variations in observed AGN luminosity (Crummy et al. 2006; Winter et al. 2012). The origins of the soft excess remain unknown; however, accretion on to an IMBH (or population of IMBH seeds) in the AGN discs could account for the luminosity and energy of the soft excess (McKernan, Ford & Reynolds 2010; McKernan et al. 2011a).

From Section 3, the innermost disc blackbody temperature for a thin disc around an IMBH of mass M_2, is $T \propto M_2^{-1/4}$, with luminosity $L \sim \eta \dot{M}_2 c^2$, where η is the accretion efficiency. For BH ($10-10^4\,{\rm M}_\odot$), $T \sim 10^7$–10^6 K (or $\sim$1–0.1 keV) and $L \sim \eta 10^{39} - 10^{42} \dot{m}_{\rm Edd}$ erg s^{-1}, where $\dot{m}_{\rm Edd}$ is the Eddington ratio. The soft X-ray excess in AGN peaks at $\sim$0.1 keV with $L_{\rm sx} \sim 10^{42-43}$ erg s^{-1} (e.g. Reynolds 1997; Winter et al. 2012). Thus, accretion on to IMBH with masses $\geq 10^4\,{\rm M}_\odot$ could account for the observed soft excess in AGN. In this model, $L_{\rm sx}$ increases as a function of M_2, $\dot{M}_2$, since from equation (6) $T_{\rm sx} \propto M_2^{1/4}\dot{M}_2^{1/4}$. Once an IMBH grows massive enough to open a gap ($q_2 \geq 10^{-4}$, depending on H/r, α), we expect $L_{\rm sx}$ to drop dramatically, unless the IMBH has an eccentric orbit (Roedig et al. 2012). In this model, AGN without a significant soft excess harbour gap-opening IMBH or very low mass IMBH.

The building blocks of IMBH in our model (nuclear cluster objects) will also accrete and generate (potentially) observable signatures. Some 10^4 white dwarfs accreting at Eddington could produce a soft X-ray spectral bump $\sim$0.03–0.05 keV (van den Heuvel et al. 1992) with luminosities $\sim 10^{42}$ erg s^{-1}. Stars embedded in the AGN disc will look similar to T-Tauri stars, emitting X-rays at $\sim 10^7$ K ($\sim$0.9 keV) but $L_{\rm x}$ is only $\sim 10^{28}$–10^{32} erg s^{-1} (Preibisch et al. 2005).

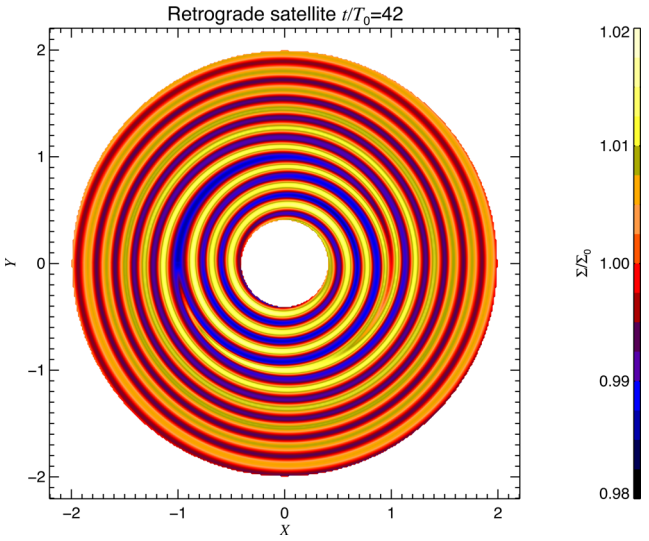

Figure 2. A 2D simulation of an NCO with mass ratio $q = 10^{-4}$ on a retrograde orbit in an isothermal, constant temperature disc of aspect ratio $H = 0.05$ in a box of dimensions $r = [0.4, 2.0]$, $\phi = [-\pi, \pi]$. An identical prograde orbiter in the same disc, after the same time, opens a prominent gap and generates spiral density waves an order of magnitude larger than those here, leading to standard type II migration.

So, even a large population ($\sim 10^5$) of T-Tauri stars in the disc would be insufficient to reproduce the AGN soft X-ray excess luminosity and a large fraction of the T-Tauri luminosity will be reprocessed as IR.

5.2 Predictions for objects on retrograde orbits

Unlike protoplanetary discs, nuclear cluster objects (NCOs, i.e. stellar mass BH, stars, stellar remnants) in AGN discs can follow retrograde orbits. Migration on to the SMBH will only occur if the retrograde NCO captures 'negative' angular momentum within its influence radius from a comparable mass of gas (e.g. Nixon et al. 2011). If most gas flows past the NCO, very little negative angular momentum will be transferred. Large-mass retrograde NCOs embedded in a disc (not in a cavity as in Nixon et al. 2011) will not open gaps because of lack of retrograde resonant torques. However, they may open a narrow annular gap as wide as their Bondi radius. Retrograde NCOs and IMBHs could persist a long time at the same AGN disc radius due to far weaker torques than predicted by standard type I and type II migration scenarios (calculated for prograde orbiters). The observational signature of retrograde objects will be the X-ray generating bow shock associated with the headwind of NCO retrograde motion.

Fig. 2 shows the results of a 2D simulation using the PENCIL CODE[1] of a satellite with mass ratio $q = 10^{-4}$ on a retrograde orbit in an isothermal, constant temperature disc of aspect ratio $H = 0.05$ in a box of dimensions $r = [0.4, 2.0]$, $\phi = [-\pi, \pi]$. From Fig. 2, the tapering spiral density waves we would expect to see in the prograde case are replaced with equal (but very small) magnitude density waves. Since the material in the tail increases by $\leq$2 per cent only over background after 42 orbits, the net torque of the gas on the retrograde NCO is far smaller than in standard (type I or II) migration scenarios, so the NCO remains at approximately the same disc radius. A bow shock caused by a star passing through a disc at relative velocity v_r will heat gas behind the shock to $T \sim 0.1 m_p v_r^2/k$ (Zentsova 1983), where m_p is the proton mass and k is Boltzmann's constant. To generate bow shocks with temperatures $\sim 0.1-1$ keV, requires relative velocities in the range $v_s \sim$ 300–1000 km s^{-1}, implying retrograde NCOs on Keplerian orbits in the outermost disc or torus ($\sim 10^{4-5} r_g$). The associated shock luminosity $L \approx \sigma A T^4 \sim 10^{42-43}$ erg s^{-1} requires the area of $\sim$20 Sun-like stars on retrograde orbits. Alternatively, the shock luminosity could be due to the single collision cross-section ($\sigma_{coll} \approx \pi r_g^2 (1 + 4GM_2/r_g v_s)$) of an $M_2 \sim 10^{3-4}$ M$_\odot$ IMBH on a retrograde orbit in the outer disc. This model of the soft X-ray excess predicts little fractional variability in the soft excess as well as a constant soft excess luminosity, independent of changes in the continuum due to accretion on to the primary SMBH. This model can be ruled out if the luminosity and variability of the soft excess and the X-ray continuum are correlated, which can be tested for a large sample of nearby AGN with *LOFT*.

5.3 Comparison with observations

The *Swift* Burst Alert Telescope (BAT) in the 14–195 keV band is unbiased towards obscured sources and host galaxy properties (e.g. Winter et al. 2012). Fig. 3 shows those AGN from the BAT sample that require a soft X-ray excess fit to the continuum (Winter et al. 2012). As we can see, the result is a scatterplot, but centred around $\sim$0.1 keV. The two dash–dotted lines in Fig. 3 correspond to our two simple models of the soft excess. The horizontal dotted line corresponds to X-ray emission due to bow shocks centred on a constant velocity of $\sim$100 km s^{-1} in the outer AGN disc, due to NCOs and IMBH on retrograde orbits. The sloping dashed line corresponds to the gap-opening threshold for an IMBH ($q \leq 2 \times 10^{-4}$, for fiducial

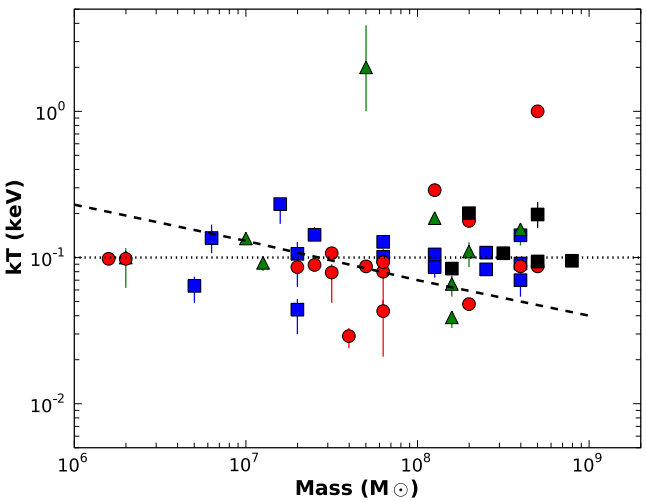

Figure 3. The peak energy (kT) of the soft X-ray excess found in AGN observed with *Swift*-BAT plotted against the mass of the central SMBH (from Winter et al. 2012). Blue squares are Seyfert 1s, black squares are broad-line radio galaxies, green triangles are Seyfert 1.2s and red circles are Seyfert 1.5s. The horizontal dotted line corresponds to a model of $\sim$0.1 keV thermal emission due to bow-shocks from NCOs/IMBH on retrograde orbits in the AGN disc, encountering 'headwinds' centred on 100 km s^{-1}. The sloping dashed line corresponds to IMBH with a constant mass ratio $q = 2 \times 10^{-4}$. Below this line, in AGN discs with fiducial $H/r = 0.05$, $\alpha = 0.01$ we expect no soft excess due to accreting IMBH (see the text).

[1] The code is publicly available under a GNU open source license and can be downloaded at http://pencil-code.googlecode.com.

disc parameters of $H/r \sim 0.05$, $\alpha \sim 0.01$) as a function of primary SMBH mass. There is substantial scatter around both model fits, but the constant temperature model is a better global fit (confirmed by a simple χ^2 test). The IMBH accretion model predicts weak or no emission from IMBH below the sloped dashed line because such objects should open a gap and decrease accretion. However, we cannot rule out this model based on Fig. 3 alone since a small factor of ∼2–3 on H/r and α, particularly in discs around lower mass SMBH, could account for soft excesses below the sloped dashed line. The retrograde orbits model can account for the range of 43/45 of the AGN in Fig. 3 if the 'median headwind' simply lies in the range 30–300 km s^{-1} (implying most NCOs/IMBH are $>10^3 r_g$ from the SMBH). In order to rule out one or both models, we need constraints from variability studies, using large effective area X-ray telescopes such as the future *LOFT* mission.

5.3.1 *Test cases: Ton S180 and future suggestions*

Constraining models of the soft excess is complicated by the presence of warm absorbing gas in AGN (McKernan, Yaqoob & Reynolds 2007). In order to distinguish between models of the soft excess, it helps to consider AGN with a soft excess but little or no warm absorption. For example, the narrow-line Seyfert galaxy Ton S180 (Veron-Cetty & Veron 2006) in a low state reveals a substantially stronger fractional variability in the softer X-rays than in hard X-rays (Nardini, Fabian & Walton 2012). In high states, the fractional variability of soft X-rays in Ton S180 appears to be similar to that of hard X-rays. In this AGN, we can rule out objects on retrograde orbits as a cause of the soft X-ray excess. If the soft excess is due to IMBH accretion, it evidently dominates emission during the low state while continuum emission dominates during the high state. However, rather than investigating individual idiosyncratic sources, it makes more sense to study a sample of AGN with soft excesses, but no warm absorption, particularly during low X-ray states where the continuum does not dominate. Observations of such a sample of AGN during 'low' states, with the large collecting area of *XMM* or future missions such as *LOFT*, will allow us to test the IMBH accretion model by comparing the variability time-scales of the soft excess and the hard X-ray continuum. The accreting IMBH model predicts that the ratio of soft excess/continuum variability time-scales during the low state is a function of the mass ratio (q) of the IMBH to the SMBH. On the one hand, competing models of the soft excess emission, such as blurred reflection (Crummy et al. 2006) can be ruled out if it can be shown that the soft excess consistently varies on shorter time-scales than the continuum. On the other hand, we can rule out the presence of luminous, accreting IMBH in AGN discs if the fractional variability of the soft excess and the hard power-law components are identical for a large sample of these AGN in 'low' X-ray states.

6 INTERMITTENT IMBH SPECTRAL SIGNATURES: PREDICTIONS

Once-off (or intermittent) observational signatures of IMBH in AGN discs or (more likely) in post-AGN galactic nuclei will be observed infrequently, but can provide strong evidence for the presence of an IMBH in a galactic nucleus. From equation (13), a 10^2 M$_\odot$ IMBH will remain orbiting a 10^6 M$_\odot$ SMBH for ∼Gyr if located $\geq 2000 r_g$. IMBH may survive the AGN phase, in the same way that Jupiter-sized planets survive protoplanetary discs. Therefore, we should expect to find IMBH in quiescent galactic nuclei (with enhanced stellar tidal disruption rates) and such IMBH may act as seeds for further growth in a new AGN phase. If IMBH are common in AGN discs (as we propose), surveys of hundreds of nearby galactic nuclei in the optical band will find the occasional event as described below.

6.1 Transits of AGN discs:predictions

An accreting IMBH in an AGN disc produces an asymmetric X-ray intensity distribution. The asymmetry of the X-ray intensity distribution may be detectable by a transit of a bloated star or optically thick cloud across the face of an AGN (see Béky & Kocsis 2012 for detailed transit calculations). The first such transit in an AGN was observed in MCG-6-30-15 (McKernan & Yaqoob 1998). This was followed by observations of transits in among others: NGC 3516 (Turner et al. 2008), NGC 1365 (Maiolino et al. 2010) and Cen A (Rivers, Markowitz & Rothschild 2011). A transit event, though rare, gives us a chance to map the AGN continuum at unprecedented resolution (<microarcseconds). If the X-ray intensity profile is asymmetric, this will show up in the best fit to the transit profile (McKernan & Yaqoob 1998). A systematic archival search of AGN X-ray light curves for transit profiles (a significant task far beyond the scope of this paper), will map the innermost accretion disc at unprecedented angular resolution and put strong limits on the occurrence of IMBH in AGN inner discs. In the optical band, transits can reveal rings of enhanced emission due to the pile-up of gas outside the orbit of a gap- or cavity-opening IMBH. Next generation space telescopes with aperture masking interferometric capabilities may be capable of detecting gaps or cavities in AGN discs (Ford et al. 2014).

6.2 QPOs and spiral density waves

Quasi-periodic oscillations are occasionally observed in AGN and a fascinating possibility is that they arise due to the action of spiral density waves in the AGN disc (Czerny et al. 2010). Depending on the disc structure, migrating IMBH should have particularly strong associated spiral density waves, analogous to those associated with migrating giant planets in protoplanetary discs (Armitage 2010). For example, a 3–4 ks QPO is observed in RE J1034 + 396 enhancing the flux by ∼5–10 per cent in the 0.3–10 keV X-ray band Czerny et al. (2010). The orbital time at $\sim 6 r_g$ around a 10^7 M$_\odot$ SMBH is ∼3ks. For a 10^5 M$_\odot$ gas disc around a $M_1 = 10^7$ M$_\odot$ SMBH, we expect ≤1 per cent or $\sim 10^3$ M$_\odot$ of gas within $10^2 r_g$ from a standard thin disc model (Sirko & Goodman 2003). If this QPO is due to spiral arms from a migrating IMBH in the AGN disc, the IMBH is $M_2 \leq 10^3$ M$_\odot$ and $a_{\rm bin} \sim 10^2 r_g$ from the SMBH. The IMBH will merge with the SMBH within $\sim 60 (10^3 \, {\rm M}_\odot / M_2)(10^7 \, {\rm M}_\odot / M_1)^2 (a_{\rm bin}/10^2 r_g)^4$ kyr. Since the corotating mass of gas at $r < 10^2 r_g$ is small, the IMBH will open a gap in the inner disc. RE J1034 + 396 is therefore a prime candidate for follow-up study of the broad component of the Fe Kα line (see Section 4 above). Post-merger, we also expect a kick on the merged object to generate a density caustic that ripples outward in a spiral wave that decays with time, but only for mass ratios $q > 10^{-2}$ (Haiman et al. 2008). A future timing mission like *LOFT* is needed in order to do a high-cadence variability study of a large sample of nearby X-ray-bright AGN. Spiral density waves raised by a migrating IMBH may show up as ripples in the broad Fe Kα line profile. Future timing studies of broad Fe Kα lines with the energy resolution and effective area of *Athena* will help constrain the location of IMBH migrators in AGN discs.

7 GWS: PREDICTIONS

Our model predicts a large number of merging NCOs and IMBH in the accretion disc around an SMBH which may be rich sources of GWs. A binary emits GWs with characteristic GW frequency (Peters & Mathews 1963)

$$f_{\rm GW} \sim \frac{(1+e)^{1/2}}{(1-e)^{3/2}}\sqrt{\frac{GM}{a^3}}\,. \tag{14}$$

The detectable GW frequency band of the planned spaced-based GW observatory *LISA*[2] or *NGO*[3] (Amaro-Seoane et al. 2011) is between 10^{-4} and 1 Hz, and between 10 and 3000 Hz for the existing Earth-based instruments LIGO[4] and VIRGO.[5] Binaries orbiting outside the last stable orbit, $a(1-e^2) \gtrsim (6+2e)\,r_{\rm g}$, are in the *LISA* (LIGO) frequency band if the total mass $M = m_1 + m_2$ is between 10^3 and 10^7 $\rm M_\odot$ (1–10^3 $\rm M_\odot$). We discuss the GW signatures of various mass sources in turn below.

7.1 GWs from an IMBH orbiting an SMBH

A compact object orbiting around a SMBH on a circular orbit emits GWs in the *LISA* band if the orbital period is less than 6 h. For SMBH mass 10^6 $\rm M_\odot$ (10^7 $\rm M_\odot$), this corresponds to an orbital radius less than 75 $r_{\rm g}$ (16 $r_{\rm g}$), or a time to merger less than 100 yr (20 yr) for an IMBH $\mu = 10^3$ $\rm M_\odot$. The signal-to-noise ratio (S/N) decreases with source distance and increases with μ as $\rm S/N \propto \mu/\mathit{D}$. The detectable distance of a circular SMBH–IMBH binary with $\rm S/N = 10$ with *LISA* is very roughly[6]

$$D_{\rm LISA} \sim 1\,{\rm Gpc}\left(\frac{M}{10^6\,{\rm M_\odot}}\right)^{-2}\frac{\mu}{10^3\,{\rm M_\odot}}\left(\frac{r}{30\,r_{\rm g}}\right)^{-4}\left(\frac{T}{1\,{\rm yr}}\right)^{1/2}, \tag{15}$$

where T is the observation time. Equation (15) implies we will detect all SMBH–IMBH mergers out to $z \sim 0.3$. The GW phase evolution may be used to independently detect and distinguish thousands of SMBH–IMBH binaries in the Universe with *LISA*, if they exist. The binary separation shrinks over time-scale $\tau_{\rm GW} \propto r^4$ given by equation (13). The relative fraction of SMBH–IMBH binaries in the Universe, that reside in a logarithmic separation interval centred at r, is proportional to $\tau_{\rm GW}$ (equation 13). Thus, most binaries will reside at large separations. However, the S/N increases towards smaller separations as r^{-4}, which implies that *LISA* will discover SMBH–IMBH binaries with a uniform probability distribution as a function of $\ln(r)$. However, at very small frequencies, the sources may constitute an unresolved GW background of 100 $\rm M_\odot$ intermediate-mass ratio inspirals (see Barack & Cutler 2004b for extreme mass ratio inspirals).

Once *LISA* detects an SMBH–IMBH binary, it can measure its physical parameters from the GW signal including the masses, separation, eccentricity, sky location and distance to the source to a level similar to SMBH–SMBH mergers. The sky localization precision is of the order of 1 $\rm deg^2$ for an SMBH–SMBH or SMBH–NCO binary approaching merger ($r \lesssim 10 r_{\rm g}$) at cosmological redshift $z = 1$ (Barack & Cutler 2004a; Lang, Hughes & Cornish 2011; Mikóczi et al. 2012), and 10 deg or more at separations $r \gtrsim 20\,r_{\rm g}$ (Kocsis et al. 2007; Lang & Hughes 2008). If the SMBH–IMBH inspirals can be identified with a similar accuracy, the 3D source localization accuracy may be sufficient to identify a unique AGN or LINER counterpart to the GW source approaching merger (Kocsis et al. 2006a). If not it will provide a 10 $\rm deg^2$ sky area for a deep triggered search for other electromagnetic signatures days to months before merger (see Kocsis et al. 2007; Kocsis, Haiman & Menou 2008). Bright AGN activity is not expected during merger if the torques of the secondary excavates a hollow cavity in the disc; instead, we expect LINER-like activity (see Section 3.3 above). However, depending on the 'leakiness' of the cavity wall, non-axisymmetric streams can supply gas to the inner regions, leading to a coincident electromagnetic counterpart (see discussion in Section 2). A precise measurement of the GW phase may also be used to look for perturbations caused by the astrophysical environment around the SMBH–IMBH binary. The *LISA* measurement accuracy is sufficient to detect the torques generated by the spiral density waves in the accretion disc if $\mu \lesssim 100\,\rm M_\odot$ (Kocsis et al. 2011; Yunes et al. 2011b).

7.2 NCOs–IMBH and IMBH–IMBH mergers

In our model, the accretion disc is expected to host abundant stellar-mass NCOs. Upon close encounters with the IMBH, these objects may become bound to the IMBH on very eccentric orbits due to GW emission (O'Leary, Kocsis & Loeb 2009). Thus, our model *predicts a new, unexpected source of GWs*. These systems generate repeated GW bursts, detectable with both LIGO and *LISA* coincidentally (Kocsis & Levin 2012). This is possible if the orbital time is less than 6 h for *LISA* detections, and the pericentre passage time-scale less than a 0.1 s for LIGO detections. As the eccentricity shrinks, the signal morphs into a continuous inspiral signal, and eventually a merger and ringdown. The detection range for LIGO and *LISA* is between 1–10 Gpc and 10 Mpc, respectively (East et al. 2013), so the odds of a coincident detection are remote.

There are no studies on the parameter estimation accuracy of repeated burst sources to date. Arguably, it should be much better than for circular sources, since these sources are in the detectable frequency band for a much longer time, the signal power is enhanced at large frequencies due to eccentricity, and these sources exhibit apsidal precession which can break parameter degeneracies (Mikóczi et al. 2012). For circular sources IMBH–NCO binaries are outside the detectable range of existing Earth-based observatories. Their detection requires the future third-generation instrument, the Einstein Telescope.[7] With the latter, circular IMBH–NCO binaries may be localized within 2 deg accuracy for $\rm S/N = 30$, the mass and distance measurement errors are 0.1 and 10 per cent, respectively (Huerta & Gair 2011).

Interestingly, the GW signal of IMBH–NCO binaries may carry information on the SMBH as well. First, the GWs are modulated by Doppler shift as the binary orbits around the SMBH (Yunes, Miller & Thornburg 2011a). Furthermore, the SMBH can secularly excite the eccentricity of the IMBH–NCO binary (Antonini & Perets 2012; Naoz et al. 2013). Since the GW signal is extremely sensitive to eccentricity (Peters & Mathews 1963), it is likely that

[2] http://lisa.nasa.gov/
[3] http://elisa-ngo.org/
[4] http://www.ligo.caltech.edu/
[5] http://www.ego-gw.it/
[6] Here, we assume that the *LISA* detector noise spectral amplitude decreases approximately as f^{-2} for $f \lesssim 10^{-3}$ Hz (Barack & Cutler 2004a), and used that the dimensionless GW strain amplitude scales as $h \propto G^2c^{-4}M\mu/(rD)$, according to the leading order quadrupolar radiation formula averaged over binary orientation. $D_{\rm LISA}$ varies by a factor 10 for $f \lesssim 10^{-2}$ Hz due to the unresolved white dwarf background and different orientations.
[7] http://www.et-gw.eu/

this perturbation would allow us to constrain the parameters of the central SMBH. This effect is the inverse of that mentioned at the end of Section 7.1. LIGO or the Einstein Telescope may measure the SMBH through its influence on the IMBH–NCO system, while *LISA* may measure the effects of an NCO through the perturbations of the SMBH–IMBH signal.

7.3 NCO–NCO scattering and capture

Finally, the NCOs which form or become captured by the accretion disc may undergo close encounters and form hard binary systems through GW emission. Hard binaries are likely IMBH seeds in AGN discs (see Paper I). For these systems, the GWs are detectable with LIGO during pericentre passage (Kocsis, Gáspár & Márka 2006b; O'Leary et al. 2009; Kocsis & Levin 2012; East et al. 2013; Samsing, MacLeod & Ramirez-Ruiz 2014). Similar to the IMBH–NCO case, the signal initially consists of repeated bursts, but transitions to a continuous eccentric inspiral in a much shorter time of minutes to days depending on the impact parameter (see equation 13 with $\mu \sim M \sim 10\ \mathrm{M}_{\odot}$).

These sources are in the LIGO frequency band before merger even in the circular case. For circular NS–NS inspirals, the source localization of the LIGO–VIRGO network is very poor 50 deg or more for S/N $\sim$ 15, but it improves to within than 10 deg with future extensions of the network through KAGRA[8] or LIGO-India[9] (Nissanke et al. 2010, 2011; Veitch et al. 2012). Similar to the IMBH–NCO case, the source localization for eccentric sources is expected to be much better. The perturbations caused by the IMBH and the SMBH may be detectable. Remarkably, NS/BH and NS/NS binaries may have coincident electromagnetic counterparts, i.e. short-hard gamma-ray bursts. The coincidence in time of an electromagnetic signal like a gamma-ray burst or the Fe Kα ripple effect allows us to locate the likely GW source.

8 CONCLUSIONS

If IMBHs can grow efficiently in AGN discs, the AGN host should exhibit myriad observational signatures. IMBHs that open gaps in AGN discs will exhibit strong observational parallels with gapped protoplanetary discs and may be detectable near merger in the broad Fe Kα line. LINER activity may be due to a weakly accreting MBH binary in a large disc cavity. If IMBHs do not open a gap, detection depends on signatures of accretion on to the IMBH (including tidal disruption events). We summarize observational signatures and compare them to current data where possible or suggest future observations.

ACKNOWLEDGEMENTS

We thank the referee for a report that helped us condense and focus this paper. We acknowledge very useful discussions with Tahir Yaqoob, Stephan Rosswog, Zoltan Haiman, Ari Laor, Hagai Perets, Kayhan Gültekin and Mordecai Mac Low. BM and KESF acknowledge support from NASA-APRA08-0117 and NSF PAARE AST-1153335. BK was supported in part by the W.M. Keck Foundation Fund of the Institute for Advanced Study and NASA grant NNX11AF29G. WL acknowledges support by the National Science Foundation under grant no. AST10-09802. This work was performed in part under contract with the California Institute of Technology (Caltech) funded by NASA through the Sagan Fellowship Program executed by the NASA Exoplanet Science Institute.

[8] http://gw.icrr.u-tokyo.ac.jp/lcgt/
[9] http://www.gw-indigo.org/tiki-index.php?page=LIGO-India

REFERENCES

Amaro-Seoane P. et al., 2012, Class. Quantum Gravit., 29, 124016
Andrews S. M., Wilner D. J., Espaillat C., Hughes A. M., Dullemond C. P., McClure M. K., Qi C., Brown J. M., 2011, ApJ, 732, 42
Antonini F., Perets H., 2012, ApJ, 757, 27
Armitage P. J., 2010, Astrophysics of Planet Formation. Cambridge Univ. Press, Cambridge
Armitage P. J., Natarajan P., 2002, ApJ, 567, L9
Artymowicz P., Lubow S. H., 1996, ApJ, 467, L77
Barack L., Cutler C., 2004a, Phys. Rev. D, 69, 082005
Barack L., Cutler C., 2004b, Phys. Rev. D, 70, 122002
Baruteau C., Ramirez-Ruiz E., Masset F., 2012, MNRAS, 423, 65
Béky B., Kocsis B., 2013, ApJ, 762, 35
Berghea C. T., Dudik R. P., 2012, ApJ, 751, 104
Bon E. et al., 2012, ApJ, 759, 118
Bryden G., Chen X., Lin D. N. C., Nelson R. P., Papaloizou J. C. B., 1999, ApJ, 514, 344
Chang P., Strubbe L. E., Menou K., Quataert E., 2010, MNRAS, 407, 2007
Collier S., Peterson B. M., 2001, ApJ, 555, 775
Crida A., Morbidelli A., Masset F., 2006, Icarus, 181, 587
Crummy J., Fabian A. C., Gallo L., Ross R. R., 2006, MNRAS, 365, 1067
Czerny B., Lachowicz P., Dovciak M., Karas V., Pechacek T., Das Tapas K., 2010, A&A, 524, A26
D'Orazio D. J., Haiman Z., MacFadyen A., 2013, MNRAS, 436, 2997
Davis S. W., Narayan R., Zhu Y., Barret D., Farrell S. A., Godet O., Servillat M., Webb N. A., 2011, ApJ, 734, 111
East W. E., McWilliams S. T., Levin J., Pretorius F., 2013, Phys. Rev. D, 87, 3004
Edgar R. G., Quillen A. C., Park J., 2007, MNRAS, 381, 1280
Eracleous M., Hwang J. A., Flohic H. M. L. G., 2010, ApJ, 711, 796
Espaillat C., Calvet N., D'Alessio P., Hernández J., Qi C., Hartmann L., Furlan E., Watson D. M., 2007, ApJ, 670, L135
Fabian A. C., Rees M. J., Stella L., White N. E., 1989, MNRAS, 238, 729
Farris B. D., Duffell P., MacFadyen A. I., Haiman Z., 2014, MNRAS, ApJ, 783, 134
Ford K. E. S., McKernan B., Sivaramakrishnan A., Martel A., Koekemoer A., Lafreniere D., Parmentier S., 2014, ApJ, 783, 73
Gierliński M., Done C., 2004, MNRAS, 349, L7
Gültekin K., Miller J. M., 2012, ApJ, 761, 90
Haiman Z., Kocsis B., Menou K., Lippai Z., Frei Z., 2008, ASP Conf. Ser. Vol. 399, Panoramic Views of Galaxy Formation and Evolution. Astron. Soc. Pac., San Francisco, p. 20
Hayasaki K., Mineshige S., Ho L. C., 2008, ApJ, 582, 1134
Ho L. C., 2008, ARA&A, 46, 475
Huerta E. A., Gair J. R., 2011, Phys. Rev. D, 83, 044021
Ivanov P. B., Papaloizou J. C. B., Polnarev A. G., 1999, MNRAS, 307, 79
Jang-Condell H., Sasselov D. D., 2003, ApJ, 593, 1116
Ju W., Greene J. E., Rafikov R. R., Bickerton S. J., Badenes C., 2013, ApJ, 777, 44
Kocsis B., Levin J., 2012, Phys. Rev. D, 85, 123005
Kocsis B., Frei Z., Haiman Z., Menou K., 2006a, ApJ, 637, 27
Kocsis B., Gáspár M. E., Márka S., 2006b, ApJ, 648, 411
Kocsis B., Haiman Z., Menou K., Frei Z., 2007, Phys. Rev. D, 76, 022003
Kocsis B., Haiman Z., Menou K., 2008, ApJ, 684, 870
Kocsis B., Yunes N., Loeb A., 2011, Phys. Rev. D, 84, 024032
Kocsis B., Haiman Z., Loeb A., 2012a, MNRAS, 427, 2660
Kocsis B., Haiman Z., Loeb A., 2012b, MNRAS, 427, 2680
Kormendy J., Richstone D., 1995, ARA&A, 33, 581
Lang R. N., Hughes S. A., 2008, ApJ, 677, 1184
Lang R. N., Hughes S. A., Cornish N. J., 2011, Phys. Rev. D, 84, 022002
Lewis K. T., Eracleous M., Storchi-Bergmann T., 2010, ApJS, 187, 416
Lin D. N. C., Papaloizou J., 1986, ApJ, 309, 846

Liu F. K., Wu X.-B., Cao S. L., 2003, MNRAS, 340, 411
McKernan B., Yaqoob T., 1998, ApJ, 501, L29
McKernan B., Yaqoob T., 2004, ApJ, 608, 157
McKernan B., Yaqoob T., Reynolds C. S., 2007, MNRAS, 379, 1359
McKernan B., Ford K. E. S., Reynolds C. S., 2010, MNRAS, 407, 2399
McKernan B., Ford K. E. S., Yaqoob T., Winter L. M., 2011a, MNRAS, 413, L24
McKernan B., Ford K. E. S., Lyra W., Perets H. B., Winter L. M., Yaqoob T., 2011b, MNRAS, 417, L103
McKernan B., Ford K. E. S., Lyra W., Perets H. B., 2012, MNRAS, 425, 460 (Paper I)
McKernan B., Ford K. E. S., Kocsis B., Haiman Z., 2013, MNRAS, 432, 1468
Maiolino R. et al., 2010, A&A, 517, 47
Maoz D., Nagar N. M., Falcke H., Wilson A. S., 2005, ApJ, 625, 699
Masset F. S., Papaloizou J. C. B., 2003, ApJ, 588, 494
Mikóczi B., Kocsis B., Forgács P., Vasúth M., 2012, Phys. Rev. D, 86, 4027
Miller M. C., Hamilton D. P., 2002, MNRAS, 330, 232
Milosavljevic M., Phinney E. S., 2005, ApJ, 622, L93
Naoz S., Kocsis B., Loeb A., Yunes N., 2013, ApJ, 773, 187
Nardini E., Fabian A. C., Walton D. J., 2012, MNRAS, 423, 3299
Nayakshin S., Sunyaev R., 2007, MNRAS, 377, 1647
Nissanke S., Holz D. E., Hughes S. A., Dalal N., Sievers J. L., 2010, ApJ, 725, 496
Nissanke S., Sievers J., Dalal N., Holz D., 2011, ApJ, 739, 99
Nixon C. J., Cossins P. J., King A. R., Pringle J. E., 2011, MNRAS, 412, 1591
O'Leary R. M., Kocsis B., Loeb A., 2009, MNRAS, 395, 2127
Pepliński A., Artymowicz P., Mellema G., 2008a, MNRAS, 386, 164
Pepliński A., Artymowicz P., Mellema G., 2008b, MNRAS, 387, 1063
Peters P. C., 1964, Phys. Rev., 136, 1224
Peters P. C., Mathews J., 1963, Phys. Rev., 131, 435
Pollack J. B., Hubickyj O., Bodenheimer P., Lissauer J. J., Podolak M., Greenzweig Y., 1996, Icarus, 124, 62
Preibisch T. et al., 2005, ApJS, 160, 401
Rafikov R. R., 2013, ApJ, 774, 144
Remillard R. A., McClintock J. E., 2006, ARA&A, 44, 49
Reynolds C. S., 1997, MNRAS, 286, 513
Rivers E., Markowitz A., Rothschild R., 2011, ApJ, 742, L29
Roedig C., Sesana A., Dotti M., Cuadra J., Amaro-Seoane P., Haardt F., 2012, A&A, 545, A127
Samsing J., MacLeod M., Ramirez-Ruiz E., 2014, ApJ, 784, 71
Scott A. E., Stewart G. C., Mateos S., 2012, MNRAS, 423, 2633
Shakura N. I., Sunyaev R. A., 1973, A&A, 24, 337
Sirko E., Goodman J., 2003, MNRAS, 341, 501
Strader J., Chomiuk L., Maccarone T. J., Miller-Jones J. C. A., Seth A. C., Heinke C. O., Sivakoff G. R., 2012, ApJ, 750, L27
Strateva I. V. et al., 2003, AJ, 126, 1720
Syer D., Clarke C. J., 1995, MNRAS, 277, 758
Turner T. J., Reeves J. N., Kraemer S. B., Miller L., 2008, A&A, 483, 161
van den Heuvel E. P. J., Bhattacharya D., Nomoto K., Rappaport S. A., 1992, A&A, 262, 97
Veitch J. et al., 2012, Phys. Rev. D, 85, 104045
Veron-Cetty M.-P., Veron P., 2006, A&A, 455, 773
Winter L. M., Veilleux S., McKernan B., Kallman T., 2012, ApJ, 745, 107
Yunes N., Miller M. C., Thornburg J., 2011a, Phys. Rev. D, 83, 044030
Yunes N., Kocsis B., Loeb A., Haiman Z., 2011b, Phys. Rev. Lett., 107, 171103
Zentsova A. S., 1983, Ap&SS, 95, 11
Zheng W. et al., 1995, ApJ, 444, 632
Zhu Z., Stone J. M., Rafikov R. R., 2013, ApJ, 768, 143

This paper has been typeset from a TEX/LATEX file prepared by the author.